Chemical Engineering Science 95 (2013) 291–300

Contents lists available at SciVerse ScienceDirect

Chemical Engineering Science

journal homepage: www.elsevier.com/locate/ces

Filtered models for scalar transport in gas–particle flows

Kapil Agrawal, William Holloway, Christian C. Milioli, Fernando E. Milioli [1], Sankaran Sundaresan *

Department of Chemical and Biological Engineering, Princeton University, Princeton, NJ 08544, USA

HIGHLIGHTS

- We develop filtered models for scalar transport in gas–particle flows.
- Model for intraphase scalar transport similar to Smagorinsky model in turbulence.
- We calculate filtered Prandtl/Schmidt numbers for each phase.
- Model for interphase scalar transport is similar to that for interphase drag.
- Orders of magnitude reduction in filtered interphase scalar transport coefficient.

ARTICLE INFO

Article history:
Received 15 December 2012
Received in revised form
2 March 2013
Accepted 11 March 2013
Available online 23 March 2013

Keywords:
Scalar transport
Fluidization
Gas–particle flow
Multiphase flow
Heat transfer
Mass transfer

ABSTRACT

We employ a kinetic-theory based two-fluid model to develop a filtered two-fluid model for scalar transport in gas–particle flows. The filtering procedure gives rise to terms describing the filtered interphase heat/mass transfer and filtered scalar diffusion, which need to be constituted in order to close the filtered transport equations. In this work, the closure for these terms is accomplished by performing fine-grid simulations of the two-fluid model in a two-dimensional periodic domain. Filtered scalar diffusion is investigated by imposing a lateral mean gradient in the scalar for each phase. Interphase energy/mass transport is investigated by prescribing a heat/species source (sink) in the solids (gas) phase, such that the energy/species content of the mixture is preserved. The variation of the filtered transport coefficients with respect to filtered particle volume fraction, and scaling with respect to filter size, filtered scalar shear rate, and filtered slip velocity is discussed. We find the filtered interphase heat transfer coefficient to be as much as two orders of magnitude smaller than the microscopic interphase heat transfer coefficient. The model for filtered scalar diffusion is found to have a form very similar to that calculated for single phase turbulent flows. We also calculate the filtered Prandtl number for each phase.

1. Introduction

Gas–particle flows are commonly encountered in the form of fluidized beds, risers, and other pneumatic conveying devices. The detailed transport behavior of these flows is frequently analyzed using continuum models in which the two phases are treated as interpenetrating continua (Gidaspow, 1994; Fan and Zhu, 1998; Jackson, 2000). High-fidelity (fine-grid) device scale simulation of the flow behavior is challenging, due to the persistent fluctuations in particle volume fraction and velocities of the two phases across a wide range of length and time scales (Agrawal et al., 2001); just as difficult is the simulation of the accompanying fluctuations in other scalar variables (e.g. species concentration, temperature). Coarse-grid simulations (employing the continuum models), while computationally tractable, are found to effectively neglect the presence of the fine-scale structure of the gas–particle flow and the associated fluctuations (Agrawal et al., 2001; Andrews et al., 2005; Igci et al., 2008), and thus the results are a poor representation of the transport behavior. A more accurate representation of the flow behavior is obtained when coarse-grid simulations employ continuum models which are modified to account for the effect of the fine-scale (sub-grid) structure of the flow (Andrews et al., 2005; Igci et al., 2008). This approach has been formulated in terms of a *filtered* two-fluid model for non-reacting gas–particle flows, where closures for the sub-grid scale fluid–particle drag force, stresses and viscosities for the two phases have been extracted from fine-grid simulations of the two-fluid model (Igci et al., 2008; Parmentier et al., 2011; Milioli et al., to appear). The first application of the same approach for reacting flows has been investigated recently (Holloway and Sundaresan, 2012).

The fine-scale structure of gas–particle flows is also found to significantly affect interphase and intraphase heat and mass

* Corresponding author. Tel.: +1 609 258 4583; fax: +1 609 258 0211.
E-mail address: sundar@princeton.edu (S. Sundaresan).
[1] Permanent address: Department of Mechanical Engineering, School of Engineering of São Carlos, University of São Paulo, Brazil.

0009-2509/$ - see front matter © 2013 Elsevier Ltd. All rights reserved.
http://dx.doi.org/10.1016/j.ces.2013.03.017

transfer. A review (Breault, 2006) of intraphase and interphase heat/mass transfer correlations (correlations for dispersion and Nusselt/Sherwood number correlations, respectively) has shown the high degree of variability and uncertainty in these correlations, and the resulting difficulty in applying them. Other studies have recognized the substantial effects of the fine-scale structure of the flowing gas–particle mixture on both interphase and intraphase heat and mass transfer and have traced the variability of the heat/mass transfer correlations to inadequate representation of the fine-scale structure of the gas–particle flow (Hansen et al., 2004; Dong et al., 2008a, 2008b; Kashyap and Gidaspow, 2010, 2011). In particular, studies have found the effective interphase heat/mass transfer rates to be diminished by several orders of magnitude (Kashyap and Gidaspow, 2010, 2011) and intraphase heat/mass transport rates to be substantially higher (Loezos and Sundaresan, 2002), as compared to the respective microscopic rates. A number of studies have attempted to model the effects of the fine-scale structure on interphase mass transfer in terms of the Energy Minimization Multiscale Method (Wang et al., 2005; Dong et al., 2008a, 2008b). The EMMS method yields constitutive models which are not dependent on the grid-resolution employed in a simulation; this is not ideal as one would expect any corrections embedded in the model to vanish as the grid resolution becomes very fine (equivalent to filter size going to zero). In the present study, our aim is to extend extant filtered two-fluid models to accommodate *passive scalar transport* in gas–particle flows. We use the term *passive scalar transport* to indicate the transport of scalar variables which do not affect the hydrodynamics: species transport within a phase and between phases, tracer transport within a phase, and energy transport within a phase and between phases. The relevance of such a model is clearly evident based on the foregoing discussion. The task will be accomplished by carrying out fine-grid simulations of gas–particle flows (with the presence of a passive scalar) in a periodic domain and filtering the results. We will calculate the filtered intraphase transport coefficient (filtered diffusivity) and filtered interphase heat/mass transfer coefficient (or equivalently the filtered Nusselt/Sherwood number correlation). It will be shown that the filtered diffusivity may be modeled using constitutive relations of the form used in large-eddy simulation of scalar transport in single phase-turbulent flows (involving the scalar shear rate associated with the respective phase velocities). Furthermore, the relationship between the filtered scalar diffusivity and filtered momentum diffusivity will be cast in terms of a filtered Prandtl/Schmidt number. The filtered interphase heat/mass transfer coefficient will be shown to have a form similar to the filtered interphase drag coefficient (but with meaningful quantitative differences). For ease of discussion in what follows, the scalar will be chosen to be the thermodynamic temperature for each phase; the results are general and apply to any passive scalar.

2. Microscopic two-fluid model equations

The two-fluid model consists of balance equations for gas- and particle-phase mass and momentum. As we employ a closure for the particle phase stress based on the kinetic theory of granular materials (Lun et al., 1984) we also require an equation for the granular temperature. We augment these equations with equations for the thermal energy balance for each phase. This set of evolution equations is presented in Table 1, along with constitutive models that close the balance equations. The constitutive models for the hydrodynamics are chosen to be consistent with earlier studies regarding filtered models within our research group (Agrawal et al., 2001; Igci et al., 2008; Holloway and Sundaresan, 2012; Milioli et al., to appear).

Table 1
Microscopic two-fluid model equations.

Evolution equations

$$\frac{\partial(\rho_s\phi_s)}{\partial t}+\nabla\cdot(\rho_s\phi_s\boldsymbol{v_s})=0 \tag{1}$$

$$\frac{\partial(\rho_g\phi_g)}{\partial t}+\nabla\cdot(\rho_g\phi_g\boldsymbol{v_g})=0 \tag{2}$$

$$\frac{\partial(\rho_s\phi_s\boldsymbol{v_s})}{\partial t}+\nabla\cdot(\rho_s\phi_s\boldsymbol{v_s}\boldsymbol{v_s})=-\phi\nabla\cdot\boldsymbol{\sigma}_g-\nabla\cdot\boldsymbol{\sigma}_s+\boldsymbol{f_D}+\rho_s\phi_s\boldsymbol{g}. \tag{3}$$

$$\frac{\partial(\rho_g\phi_g\boldsymbol{v_g})}{\partial t}+\nabla\cdot(\rho_g\phi_g\boldsymbol{v_g}\boldsymbol{v_g})=-\phi_g\nabla\cdot\boldsymbol{\sigma}_g-\boldsymbol{f_D}+\rho_g\phi_g\boldsymbol{g} \tag{4}$$

$$\frac{3}{2}\left[\frac{\partial(\rho_s\phi_s\theta)}{\partial t}+\nabla\cdot(\rho_s\phi_s\theta\boldsymbol{v_s})\right]=-\nabla\cdot\boldsymbol{q}-\boldsymbol{\sigma}_s:\nabla\boldsymbol{v_s}-J_{\text{vis}}-J_{\text{coll}}+\Gamma_{\text{slip}} \tag{5}$$

$$\frac{\partial(\rho_sC_{p_s}\phi_sT_s)}{\partial t}+\nabla\cdot(\rho_sC_{p_s}\phi_sT_s\boldsymbol{v_s})=\nabla\cdot(k_s\phi_s\nabla T_s)+I_T \tag{6}$$

$$\frac{\partial(\rho_gC_{p_g}\phi_gT_g)}{\partial t}+\nabla\cdot(\rho_gC_{p_g}\phi_gT_g\boldsymbol{v_g})=\nabla\cdot(k_g^*\phi_g\nabla T_g)-I_T \tag{7}$$

Closures

Gas phase stress tensor ($\boldsymbol{\sigma}_g$)

$$\boldsymbol{\sigma}_g=p_g\boldsymbol{I}-\mu_g^*(\nabla\boldsymbol{v_g}+(\nabla\boldsymbol{v_g})^T-\tfrac{2}{3}(\nabla\cdot\boldsymbol{v_g})\boldsymbol{I}) \tag{8}$$

Solid phase stress tensor ($\boldsymbol{\sigma}_s$)

$$\boldsymbol{\sigma}_s=(\rho_s\phi_s(1+4\phi_sg_0)\theta-\eta\mu_b(\nabla\cdot\boldsymbol{v_s}))\boldsymbol{I}-2\mu_s\boldsymbol{S},\quad \eta=\frac{1+e_p}{2}, \tag{9}$$

$$g_0=\frac{1}{1-(\phi_s/\phi_{s_{max}})^{1/3}},\quad \mu_b=\frac{256\mu\phi_s^2g_0}{5\pi},\quad \mu=\frac{5\rho_sd\sqrt{\pi\theta}}{96}, \tag{10}$$

$$\mu_s=\frac{1.2\mu^*}{g_0\eta(2-\eta)}\left(1+\frac{8}{5}\phi_s\eta g_0\right)\left(1+\frac{8}{5}\eta(3\eta-2)\phi_sg_0+\frac{6}{5}\eta\mu_b\right), \tag{11}$$

$$\mu^*=\frac{\mu}{1+\dfrac{2\beta\mu}{(\rho_s\phi_s)^2g_0\theta}},\quad \boldsymbol{S}=\frac{1}{2}(\nabla\boldsymbol{v_s}+(\nabla\boldsymbol{v_s})^T)-\frac{1}{3}(\nabla\cdot\boldsymbol{v_s})\boldsymbol{I}. \tag{12}$$

Fluid-particle drag force ($\boldsymbol{f_D}$)

$$\boldsymbol{f_D}=\beta(\boldsymbol{v_g}-\boldsymbol{v_s}),\quad \beta=\frac{C_D}{d^2}Re_g\phi_s\mu_g^*\phi_g^{-2.65},\quad Re_g=\frac{\phi_g\rho_gd|\boldsymbol{v_g}-\boldsymbol{v_s}|}{\mu_g^*} \tag{13}$$

$$C_D=\frac{18}{Re_g}(1+0.15Re_g^{0.687}),Re_g<1000;\quad 0.33,\ Re_g\geq1000 \tag{14}$$

Diffusive flux of granular energy ($\boldsymbol{q}$)

$$\boldsymbol{q}=-\lambda\nabla\theta \tag{15}$$

$$\lambda=\frac{\lambda^*}{g_0}\left(\left(1+\frac{12}{5}\eta\phi_sg_0\right)\left(1+\frac{12}{5}\eta^2(4\eta-3)\phi_sg_0\right)+\frac{64}{25\pi}(41-33\eta)\eta^2\phi_s^2g_0^2\right) \tag{16}$$

$$\lambda^*=\frac{\lambda_i}{1+\dfrac{6\beta\lambda_i}{5(\rho_s\phi_s)^2g_0\theta}};\quad \lambda_i=\frac{75\rho_sd\sqrt{\pi\theta}}{48\eta(41-33\eta)} \tag{17}$$

Dissipation of granular energy via inelastic collisions (J_{coll})

$$J_{\text{coll}}=\frac{48}{\sqrt{\pi}}\eta(1-\eta)\frac{\rho_s\phi_s^2}{d}g_0\theta^{3/2} \tag{18}$$

Dissipation of granular energy via viscous action of the fluid phase (J_{vis})

$$J_{\text{vis}}=\frac{54\phi_s\mu_g^*\theta}{d^2}R_{diss} \tag{19}$$

$$R_{diss}=1+3\sqrt{\frac{\phi_s}{2}}+\frac{135}{64}\phi_s\ln(\phi_s)+11.26\phi_s(1-5.1\phi_s+16.57\phi_s^2-21.77\phi_s^3)-\phi_sg_0\ln(0.01) \tag{20}$$

Production of granular energy through slip between phases (Γ_{slip})

$$\Gamma_{\text{slip}}=\frac{81\phi\mu_g^{(*)2}|\boldsymbol{u}-\boldsymbol{v}|^2}{g_0d^3\rho_g\sqrt{\pi\theta}}\frac{R_{drag}^2}{1+3.5\sqrt{\phi_s}+5.9\phi_s} \tag{21}$$

$$R_{drag}=\frac{1+3\sqrt{\phi_s/2}+(135/64)\phi_s\ln(\phi_s)+17.14\phi_s}{1+0.681\phi_s-8.48\phi_s^2+8.16\phi_s^3},\quad \phi_s<0.40;\frac{10\phi_s}{(1-\phi_s)^3}+0.7,\quad \phi_s\geq0.40 \tag{22}$$

Effective thermal conductivity of particle phase k_s

$$k_s=\frac{\rho_sC_{p_s}d\pi^{3/2}\sqrt{\theta}}{32g_0} \tag{23}$$

Interphase heat transfer I_T

$$I_T=\gamma(T_s-T_g);\quad \gamma=\frac{6k_g^*\phi_sNu}{d^2} \tag{24}$$

Table 1 (*continued*)

$$Nu = (7-10\phi_g+5\phi_g^2)(1+0.7Re_g^{0.2}Pr_g^{1/3})+(1.33-2.4\phi_g+1.2\phi_g^2)Re_g^{0.7}Pr_g^{1/3} \quad (25)$$

$$Pr_g = \frac{C_{p_g}\mu_g^*}{k_g^*} \quad (26)$$

The effective gas-phase conductivity, k_g^* and effective gas-phase viscosity μ_g^* appearing in Eqs. (7) and (8) will typically differ from the corresponding molecular properties as they should account for the enhanced scalar and momentum transport that results from additional pseudo-turbulent transport occurring as a result of microscopic interactions between individual particles and the fluid. However, two-fluid model simulations have revealed that the filtered solutions of the two-fluid model are quite insensitive to the value of μ_g^* (Agrawal et al., 2001). Therefore, we set μ_g^* equal to the molecular viscosity μ_g. In addition, the effective gas-phase conductivity k_g^* is set to the bulk molecular conductivity, k_g. The expression for the conductivity k_s of the particle phase is determined by applying the kinetic theory of granular materials, and is given in Eq. (23) (Hsiau and Hunt, 1993; Hunt, 1997; Schmidt and Renz, 2000). The term involving interphase heat transfer requires the specification of a Nusselt number correlation. We employ the correlation developed by Gunn (1978), which is shown in Eq. (25).

3. Filtered two-fluid model equations

The filtered two-fluid model equations are obtained by performing a spatial average of the microscopic two-fluid model equations. As a result of the filtering procedure, the effect of the fine-scale gas–particle flow structure occurring on length scales smaller than the filter size is captured through residual terms that must be constituted from theoretical considerations or from filtering the results of fine-grid two-fluid model simulations. Filtered models have been shown to yield quantitatively similar macroscopic behavior to that observed in fine-grid simulations of the same (Igci and Sundaresan, 2011a). The filtering procedure we adopt is that employed by Igci et al. (2008).

Given the particle volume fraction $\phi_s(\boldsymbol{y},t)$ at location $\boldsymbol{y}$ and time t, we define the filtered particle volume fraction $\overline{\phi_s}(\boldsymbol{x},t)$ as

$$\overline{\phi_s}(\boldsymbol{x},t) = \int_{V_\infty} G(\boldsymbol{x},\boldsymbol{y})\phi_s(\boldsymbol{y},t)\,d\boldsymbol{y} \quad (27)$$

where $G(\boldsymbol{x},\boldsymbol{y})$ is a weight function which is a function of $\boldsymbol{x}-\boldsymbol{y}$ and V_∞ denotes the region in which the gas–particle flow occurs. We require that $\int_{V_\infty} G(\boldsymbol{x},\boldsymbol{y})\,d\boldsymbol{y}=1$; in this study we use a top hat filter for $G(\boldsymbol{x},\boldsymbol{y})$. The filtered velocities and temperatures of the two phases are defined as

$$\overline{\phi_s}(\boldsymbol{x},t)\widetilde{\boldsymbol{v}_s}(\boldsymbol{x},t) = \int_{V_\infty} G(\boldsymbol{x},\boldsymbol{y})\phi_s(\boldsymbol{y},t)\boldsymbol{v_s}(\boldsymbol{y},t)\,d\boldsymbol{y} \quad (28)$$

$$\overline{\phi_g}(\boldsymbol{x},t)\widetilde{\boldsymbol{v}_g}(\boldsymbol{x},t) = \int_{V_\infty} G(\boldsymbol{x},\boldsymbol{y})\phi_g(\boldsymbol{y},t)\boldsymbol{v_g}(\boldsymbol{y},t)\,d\boldsymbol{y} \quad (29)$$

$$\overline{\phi_s}(\boldsymbol{x},t)\widetilde{T_s}(\boldsymbol{x},t) = \int_{V_\infty} G(\boldsymbol{x},\boldsymbol{y})\phi_s(\boldsymbol{y},t)T_s(\boldsymbol{y},t)\,d\boldsymbol{y} \quad (30)$$

$$\overline{\phi_g}(\boldsymbol{x},t)\widetilde{T_g}(\boldsymbol{x},t) = \int_{V_\infty} G(\boldsymbol{x},\boldsymbol{y})\phi_g(\boldsymbol{y},t)T_g(\boldsymbol{y},t)\,d\boldsymbol{y} \quad (31)$$

We define the filtered scalar shear rate for the two phases as follows:

$$s_i = \sqrt{2\widetilde{\boldsymbol{S}}_i:\widetilde{\boldsymbol{S}}_i}, \quad i=s,g \quad (32)$$

For each of the variables above, we define a corresponding fluctuating variable as follows:

$$\phi'_s(\boldsymbol{y},t) = \phi_s(\boldsymbol{y},t)-\overline{\phi_s}(\boldsymbol{y},t) \quad (33)$$

$$\boldsymbol{v'_s}(\boldsymbol{y},t) = \boldsymbol{v_s}(\boldsymbol{y},t)-\widetilde{\boldsymbol{v_s}}(\boldsymbol{y},t) \quad (34)$$

$$\boldsymbol{v'_g}(\boldsymbol{y},t) = \boldsymbol{v_g}(\boldsymbol{y},t)-\widetilde{\boldsymbol{v_g}}(\boldsymbol{y},t) \quad (35)$$

$$T'_s(\boldsymbol{y},t) = T_s(\boldsymbol{y},t)-\widetilde{T_s}(\boldsymbol{y},t) \quad (36)$$

$$T'_g(\boldsymbol{y},t) = T_g(\boldsymbol{y},t)-\widetilde{T_g}(\boldsymbol{y},t) \quad (37)$$

The filtered mass and momentum balance equations remain unchanged from those derived in the work of Igci et al. (2008), and we refer the reader to the same.

Of interest are the filtered thermal energy balance equations; invoking the above definitions of filtered and fluctuating variables we find

$$\rho_s C_{p_s}\left[\frac{\partial(\overline{\phi_s}\widetilde{T_s})}{\partial t}+\nabla\cdot(\overline{\phi_s}\widetilde{\boldsymbol{v_s}}\widetilde{T_s})\right] = \nabla\cdot(\overline{k_s\phi_s\nabla T_s}) + \overline{\gamma(T_s-T_g)}-\rho_s C_{p_s}\nabla\cdot(\phi_s\widetilde{\boldsymbol{v'_s}T'_s}) \quad (38)$$

$$\rho_g C_{p_g}\left[\frac{\partial(\overline{\phi_g}\widetilde{T_g})}{\partial t}+\nabla\cdot(\overline{\phi_g}\widetilde{\boldsymbol{v_g}}\widetilde{T_g})\right] = \nabla\cdot(\overline{k_g\phi_g\nabla T_g}) - \overline{\gamma(T_s-T_g)}-\rho_g C_{p_g}\nabla\cdot(\phi_s\widetilde{\boldsymbol{v'_g}T'_g}) \quad (39)$$

The left hand side of the filtered thermal energy balances resembles the unfiltered microscopic equation, with the unfiltered variables replaced by their filtered counterparts. The second term on the right hand side represents filtered interphase energy transport while the quantities in the last term on the right hand side of both equations are dispersive terms that may be modeled as a diffusive flux. The filtered interphase heat transfer coefficient may be defined as

$$\gamma_{filt} = \frac{\overline{\gamma(T_s-T_g)}}{(\widetilde{T_s}-\widetilde{T_g})} \quad (40)$$

We define the filtered thermal diffusivities as follows:

$$\alpha_{s_{filt}}\nabla\widetilde{T_s} = -\phi_s\widetilde{\boldsymbol{v'_s}T'_s}, \quad \alpha_{g_{filt}}\nabla\widetilde{T_g} = -\phi_g\widetilde{\boldsymbol{v'_g}T'_g} \quad (41)$$

4. Simulation procedure

Following earlier studies by Igci et al. (2008), we simulate a fluidized gas–particle system in a two-dimensional periodic domain; the vertical pressure drop in the gas phase is set to balance the weight of the mixture. The microscopic equations are implemented in MFIX (Syamlal et al., 1993).

In order to facilitate the calculation of the filtered thermal diffusivity, we employ a procedure commonly employed in the simulation of scalar transport in single phase turbulent flows; we impose a mean lateral temperature gradient, ξ, in each of the two phases (Moin et al., 1991; Rogers et al., 1989). The temperatures of the two phases are decomposed as follows:

$$T_s = T_s^* + \xi x; \quad T_g = T_g^* + \xi x; \quad \xi = constant \quad (42)$$

The microscopic thermal energy balances now have the following form:

$$\frac{\partial(\rho_s C_{p_s}\phi_s T_s^*)}{\partial t}+\nabla\cdot(\rho_s C_{p_s}\phi_s T_s^*\boldsymbol{v_s}) = \nabla\cdot(k_s\phi_s\nabla T_s^*) + \gamma(T_s^*-T_g^*)+\xi\frac{\partial(k_s\phi_s)}{\partial x}-\rho_s C_{p_s}\phi_s v_{s_x}\xi \quad (43)$$

$$\frac{\partial(\rho_g C_{p_g}\phi_g T_g^*)}{\partial t}+\nabla\cdot(\rho_g C_{p_g}\phi_g T_g^*\boldsymbol{v_g}) = \nabla\cdot(k_g\phi_g\nabla T_g^*)$$

Table 2
Typical values of physical parameters for particle and gas phases.

Particle diameter	d	7.5×10^{-5} m
Particle density	ρ_s	1500 kg/m^3
Gas density	ρ_g	1.3 kg/m^3
Gas molecular viscosity	μ_g	1.8×10^{-5} kg/(m s)
Gas molecular conductivity	k_g	0.024 W/(m K)
Gas heat capacity	C_{p_g}	1.15×10^{3} J/(Kg K)
Particle heat capacity	C_{p_s}	1×10^{3} J/(Kg K)
Coefficient of restitution	e_p	0.9
Terminal settling velocity	v_t	0.2184 m/s

$$-\gamma(T_s^*-T_g^*)+\xi\frac{\partial(k_g\phi_s)}{\partial x}-\rho_g C_{p_g}\phi_g v_{g_x}\xi \tag{44}$$

The equations are the same as those in Table 1, with the addition of the last two terms in each equation: these represent source terms. The subscript x on the velocity indicates the lateral component of the phase velocity. The modified thermal energy balance equations given by Eqs. (43) and (44) replace those in Table 1 for the purposes of calculating the filtered thermal diffusivities. Even though we will present results in dimensionless form, it is useful to consider a typical physical system to motivate the computations (see Table 2). For such a physical system we set the lateral temperature gradient, ξ, to be 1 °C/cm; the results are not sensitive to the value of this parameter. Using this specification we will be able to calculate the lateral component of the thermal diffusivity (the vertical/axial transport is dominated by convection).

In order to facilitate the calculation of the filtered interphase heat transfer coefficient we construct a system in which there is a persistent difference in filtered temperature of the two phases, leading to a persistent interphase filtered heat flux. We accomplish this by introducing a heat source in the particle phase and a heat sink in the gas phase, such that the mixture energy content is preserved. The local heat source in the particle phase is set to

$$\dot{\Pi}_s\phi_s \tag{45}$$

where $\dot{\Pi}_s$ is a constant and is the rate of energy input in the particle phase. In order for the mixture energy content to be preserved we set the heat sink in the gas phase to be

$$\dot{\Pi}_g\phi_g=\dot{\Pi}_s\frac{\langle\phi_s\rangle_d}{\langle\phi_g\rangle_d}\phi_g \tag{46}$$

where $\langle\phi_s\rangle_d$ is the domain-averaged particle phase volume fraction (averaged over the computational domain), and is a constant. The microscopic thermal energy balances now have the following form:

$$\frac{\partial(\rho_s C_{p_s}\phi_s T_s)}{\partial t}+\nabla\cdot(\rho_s C_{p_s}\phi_s T_s\boldsymbol{v_s})=\nabla\cdot(k_s\phi_s\nabla T_s)+\gamma(T_s-T_g)+\dot{\Pi}_s\phi_s \tag{47}$$

$$\frac{\partial(\rho_g C_{p_g}\phi_g T_g)}{\partial t}+\nabla\cdot(\rho_g C_{p_g}\phi_g T_g\boldsymbol{v_g})=\nabla\cdot(k_g^*\phi_g\nabla T_g)-\gamma(T_s-T_g)-\dot{\Pi}_s\frac{\langle\phi_s\rangle_d}{\langle\phi_g\rangle_d}\phi_g \tag{48}$$

The equations are the same as those in Table 1, with the addition of the last terms in each equation: these represent the source/sink terms. The modified thermal energy balances given by Eqs. (47) and (48) replace those in Table 1 for the purposes of calculating the filtered interphase heat transfer coefficient. In our simulations we set $\dot{\Pi}_s$ such that the heating rate of the particle phase is 0.1 °C/s; the results are not sensitive to the value of this parameter.

We simulate the gas–particle system in a 32 cm × 32 cm computational domain for values of $\langle\phi_s\rangle_d$ ranging from 0.01 to 0.55. In order to show the effect of grid resolution, two grid resolutions are used: $\delta=1.25$ mm and $\delta=2.5$ mm (it will be shown in later sections that both resolutions give nearly the same results and as such we consider convergence with respect to grid resolution sufficient at $\delta=1.25$ mm. Unless otherwise stated, the grid resolution is $\delta=1.25$ mm.) All calculations in this study are performed for FCC catalyst particles fluidized by air; the corresponding values for the physical properties are given in Table 2.[2] Simulations are initiated from a slightly non-uniform state to facilitate the rapid development of inhomogeneous flow structures. After an initial transient period, the system reaches a statistical steady state with persistent temporally and spatially inhomogeneous structures. Snapshots of the flow field are collected at various times in this statistical steady state (See Fig. 2 in Igci et al. (2008) for a sample snapshot). These computational data are then filtered using filters of different sizes (Δ) and "binned" with respect to the filtered particle phase volume fraction, $\overline{\phi_s}$, the magnitude of the filtered slip velocity, $|\widetilde{\boldsymbol{v_s}}-\widetilde{\boldsymbol{v_g}}|$, and the filtered scalar shear rates $\hat{s}_s$ and $\hat{s}_g$, as appropriate. Next the data are ensemble-averaged within each bin in order to collect sufficient statistics of filtered quantities. Further details of the procedure for this filtering operation can be found in Igci et al. (2008).

We employ the particle density (ρ_s), the terminal settling velocity of an isolated particle (v_t), and gravitational acceleration ($|\boldsymbol{g}|$), as the characteristic density, velocity and acceleration scales to non-dimensionalize all results presented in this work. The dimensionless filtered quantities of interest are

$$\hat{\Delta}=\Delta\frac{|\boldsymbol{g}|}{v_t^2};\quad \hat{\widetilde{\boldsymbol{v}}}_i=\frac{\widetilde{\boldsymbol{v}}_i}{v_t};\quad \hat{\widetilde{s}}_i=\widetilde{s}_i\frac{v_t}{|\boldsymbol{g}|};\quad \hat{\alpha}_{i_{\hat{f}ilt}}=\alpha_{i_{\hat{f}ilt}}\frac{|\boldsymbol{g}|}{v_t^3};\quad i=s,g \tag{49}$$

The dimensionless slip velocity is written as $|\hat{\widetilde{\boldsymbol{v}}}_s-\hat{\widetilde{\boldsymbol{v}}}_g|$.

Before we present the simulation results, it is appropriate to discuss the manner in which the results obtained here may be applied to real systems, which are not periodic and are wall-bounded. Prior simulations on wall-bounded riser flows and those in fully periodic domains have revealed that in regions away from the riser walls (i.e., the core region), the statistics obtained from the period domain simulations and those obtained from the wall-bounded case are quite similar. The same set of simulations revealed that in regions close to the walls, the statistics exhibited appreciable departure from those obtained via periodic domain simulations, and as such the constitutive models obtained for the same required adjustment. These adjustments are discussed in Igci and Sundaresan (2011a), wherein the constitutive models for the meso-scale stresses were based on a scaling with v_t^2. Strictly speaking, changing the models to those based on the scalar shear rate (as will be seen in the next section), does not remove the need for wall corrections. However, we anticipate that by following the test filter approach of Germano et al. (1991), which has been applied to gas–particle flows by Parmentier et al. (2011), we may capture the wall corrections at least partially without further empiricism. The efficacy of this approach remains to be demonstrated.

[2] At a much earlier stage in our studies aimed at developing filtered models, we performed simulations for particles with different particle size, leading to terminal velocities (v_t) ranging from about 10 cm/s to 50 cm/s. It was found that the results obtained with different particles could be collapsed reasonably well by using v_t as the characteristic velocity and v_t^2/g as the characteristic length (see Igci, 2011). Therefore, in the present study, we have performed simulations corresponding to one v_t and have scaled the results using the aforementioned characteristic velocity and length scales. This is equivalent to making the problem dimensionless and then solving it. However, we also discuss dimensional quantities in the paper for a typical particle size encountered in many fluidized beds to make it easier to explain the application to real systems.

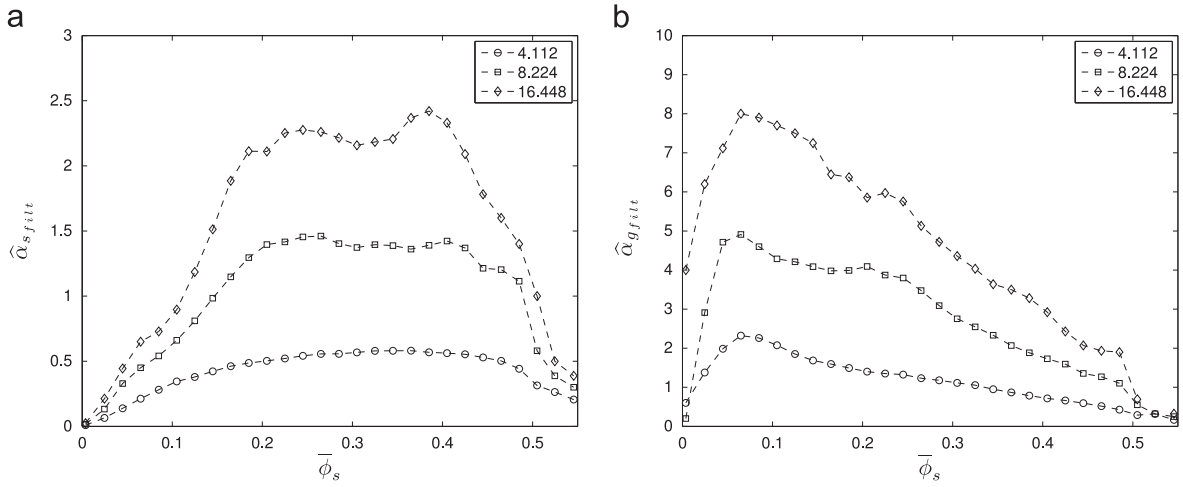

Fig. 1. Dimensionless filtered thermal diffusivity as a function of filtered particle volume fraction for different filter sizes. Legend indicates dimensionless filter size. (a) particle phase and (b) gas phase.

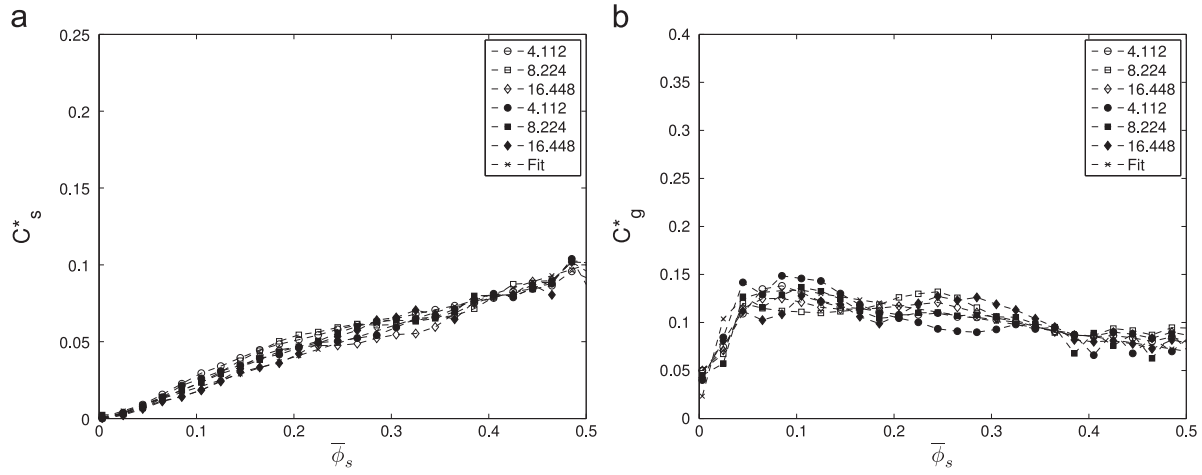

Fig. 2. Dimensionless filtered thermal diffusivity coefficient as a function of filtered particle volume fraction for different filter sizes. Legend indicates dimensionless filter size. Open/filled symbols correspond to a grid resolution of 1.25 mm/2.5 mm. The dashed line with 'x' marker symbol is a fit to the data. (a) particle phase and (b) gas phase.

5. Results for filtered thermal diffusivity

Fig. 1a and b presents the variation of the $\hat{\alpha}_{s_{filt}}$ and $\hat{\alpha}_{g_{filt}}$ with respect to the filtered particle phase volume fraction, $\overline{\phi_s}$ for different filter sizes. The dependence of the filtered thermal diffusivities is very similar to that of the filtered viscosities for the two phases (see Igci et al., 2008; Milioli et al., to appear); the filtered transport properties go to zero in the limit of low and high particle volume fraction, and there is a substantial dependence on the filter size. Milioli et al. (to appear) show that the filtered viscosities of the two phases may be reasonably modeled using a Smagorinsky type model (Smagorinsky, 1963; Pope, 2000), when the dependency is cast in terms of the respective scalar shear rates, filter size, and the filtered particle phase volume fraction. We should expect similar behavior for the filtered thermal diffusivities. We write

$$\hat{\alpha}_{i_{filt}} = C_i^* \hat{\Delta}^2 \hat{\bar{s}}_i \quad i = s,g \tag{50}$$

Fig. 2a and b shows the variation of the coefficient C_i^* for the particle and gas phase (and the fit thereto), respectively. The results for two different grid resolutions are shown ($\delta = 1.25/2.5$ mm). We observe that the dependency with respect to the filter size is removed with the above specification of the $\hat{\alpha}_{i_{filt}}$. The resemblance to a Smagorinsky type model for thermal diffusivity (Moin et al., 1991) is evident, except that the coefficients C_i^* are a function of $\overline{\phi_s}$. In particular we propose the following fits:

$$C_s^* = 0.21\overline{\phi_s}; \quad C_g^* = \begin{cases} 0.134(1-e^{-60\overline{\phi_s}}) & \overline{\phi_s} < 0.1 \\ 0.15-0.16\overline{\phi_s} & \overline{\phi_s} \geq 0.1 \end{cases} \tag{51}$$

Comparing the fit for the coefficients with the analogous ones for the filtered viscosities (see Milioli et al., to appear) we may calculate the filtered Prandtl number for each phase

$$Pr_{s_{filt}} \equiv \frac{\hat{\nu}_{s_{filt}}}{\hat{\alpha}_{s_{filt}}} = 0.5; \quad Pr_{g_{filt}} \equiv \frac{\hat{\nu}_{g_{filt}}}{\hat{\alpha}_{g_{filt}}} = \frac{0.17-0.275\overline{\phi_s}}{0.15-0.16\overline{\phi_s}}, \quad \overline{\phi_s} \geq 0.1 \tag{52}$$

Note that while C_g^* rapidly approaches zero as $\overline{\phi_s} \to 0$, Milioli et al. (to appear) do not report similar behavior for the analogous coefficient for the filtered gas phase viscosity, as such we report $Pr_{g_{filt}}$ only for $\overline{\phi_s} \geq 0.1$. While $Pr_{s_{filt}}$ is constant at 0.5, $Pr_{g_{filt}}$ varies between 0.5 and 1; the reason for the different behavior for the two phases is not readily apparent and merits further investigation. In any case the range of the observed filtered Prandtl numbers is not dissimilar to what is seen in single phase turbulent flows (Moin et al., 1991; Rogers et al., 1989). When implementing filtered two-fluid models we may directly specify the filtered thermal diffusivities or alternatively specify the filtered Prandtl numbers.

The results we have just discussed are in the case where interphase transport is permitted. We have also examined the case of a passive scalar which is restricted to a given phase (such as a tracer). These results are shown in Fig. 3a and b; the presence of

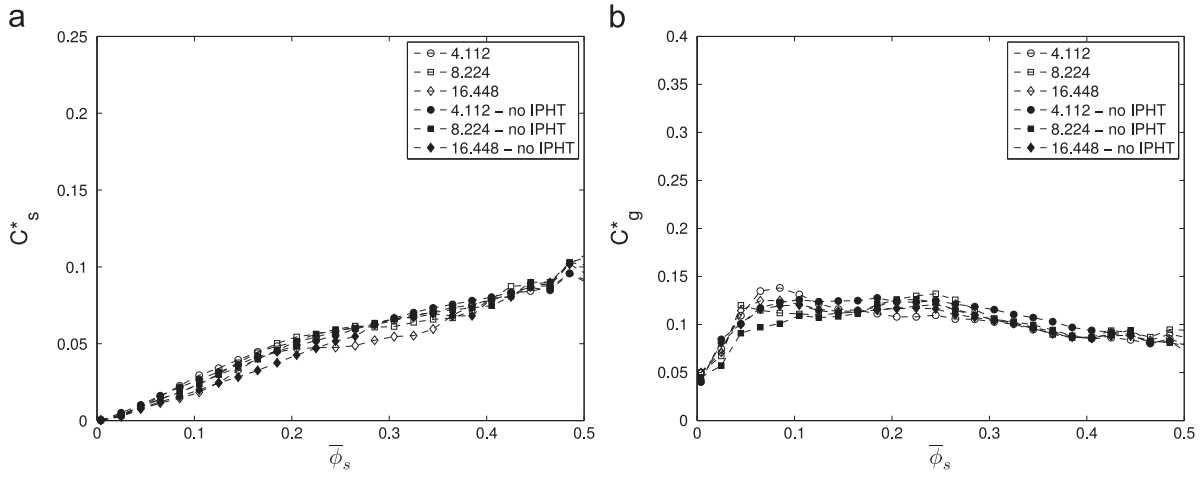

Fig. 3. Dimensionless filtered thermal diffusivity coefficient as a function of filtered particle volume fraction for different filter sizes. Legend indicates dimensionless filter size. Filled symbols correspond to the case where interphase heat transfer is not permitted. (a) particle phase and (b) gas phase.

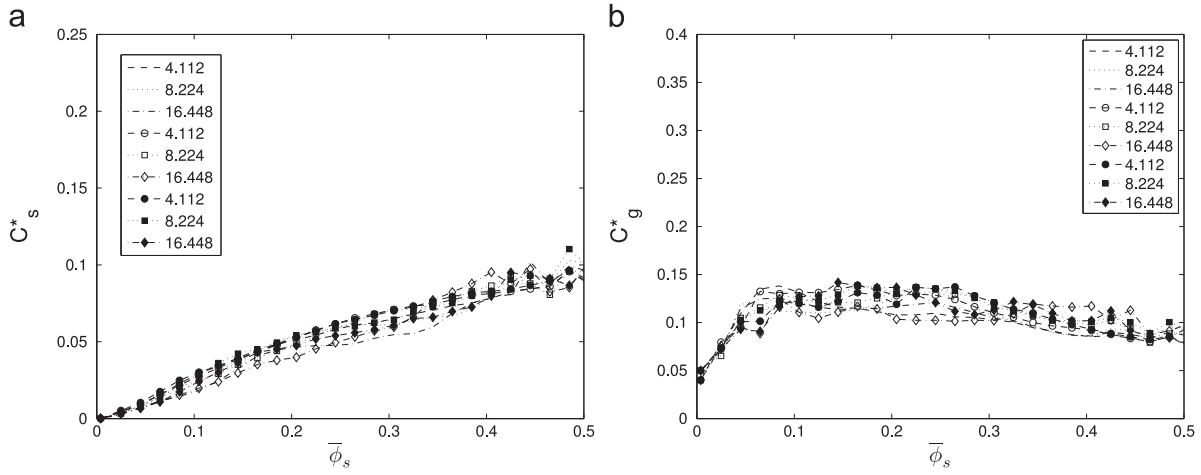

Fig. 4. Dimensionless filtered thermal diffusivity coefficient as a function of filtered particle volume fraction for different filter sizes. Legend indicates dimensionless filter size. Dashed lines without symbols corresponds to $e_p = 0.9$. Open/filled symbols correspond to $e_p = 0.85/0.95$. (a) particle phase and (b) gas phase.

interphase transfer of a scalar, or lack thereof, does not appear to influence the filtered diffusivities.

Finally, we examine the effect of varying the coefficient of restitution on the filtered diffusivities, shown in Fig. 4a and b. The results show negligible sensitivity over the typical range of values chosen for the coefficient of restitution.

6. Results for filtered interphase heat transfer coefficient

We define the correction to the interphase heat transfer coefficient, Q, as follows:

$$Q = 1 - \frac{\gamma_{filt}}{\gamma(\overline{\phi_s}, |\widetilde{\boldsymbol{v}}_s - \widetilde{\boldsymbol{v}}_g|)} \tag{53}$$

A value of zero, for the correction, Q, essentially implies a homogeneous fine-scale (sub-filter scale) microstructure, while increasingly larger values of Q imply an increasingly heterogeneous fine-scale microstructure. Fig. 5 shows a scatter plot of the correction, Q. Each point corresponds to a specific combination of $\overline{\phi_s}$, $|\widetilde{\boldsymbol{v}}_s - \widetilde{\boldsymbol{v}}_g|$, and $\hat{\Delta}$, and represents the average of a large number of realizations. The dimensionless filter size, $\hat{\Delta}$,

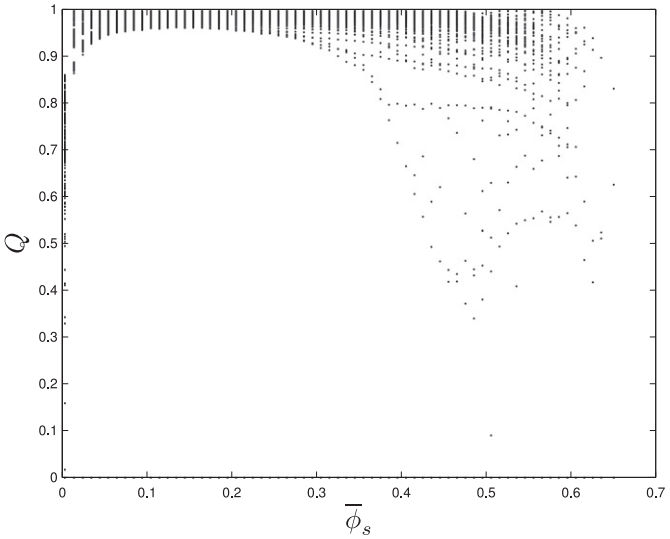

Fig. 5. Scatter plot of the correction to the interphase heat transfer coefficient, Q. Each point corresponds to a specific combination of $\overline{\phi_s}$, $|\widetilde{\boldsymbol{v}}_s - \widetilde{\boldsymbol{v}}_g|$, and $\hat{\Delta}$.

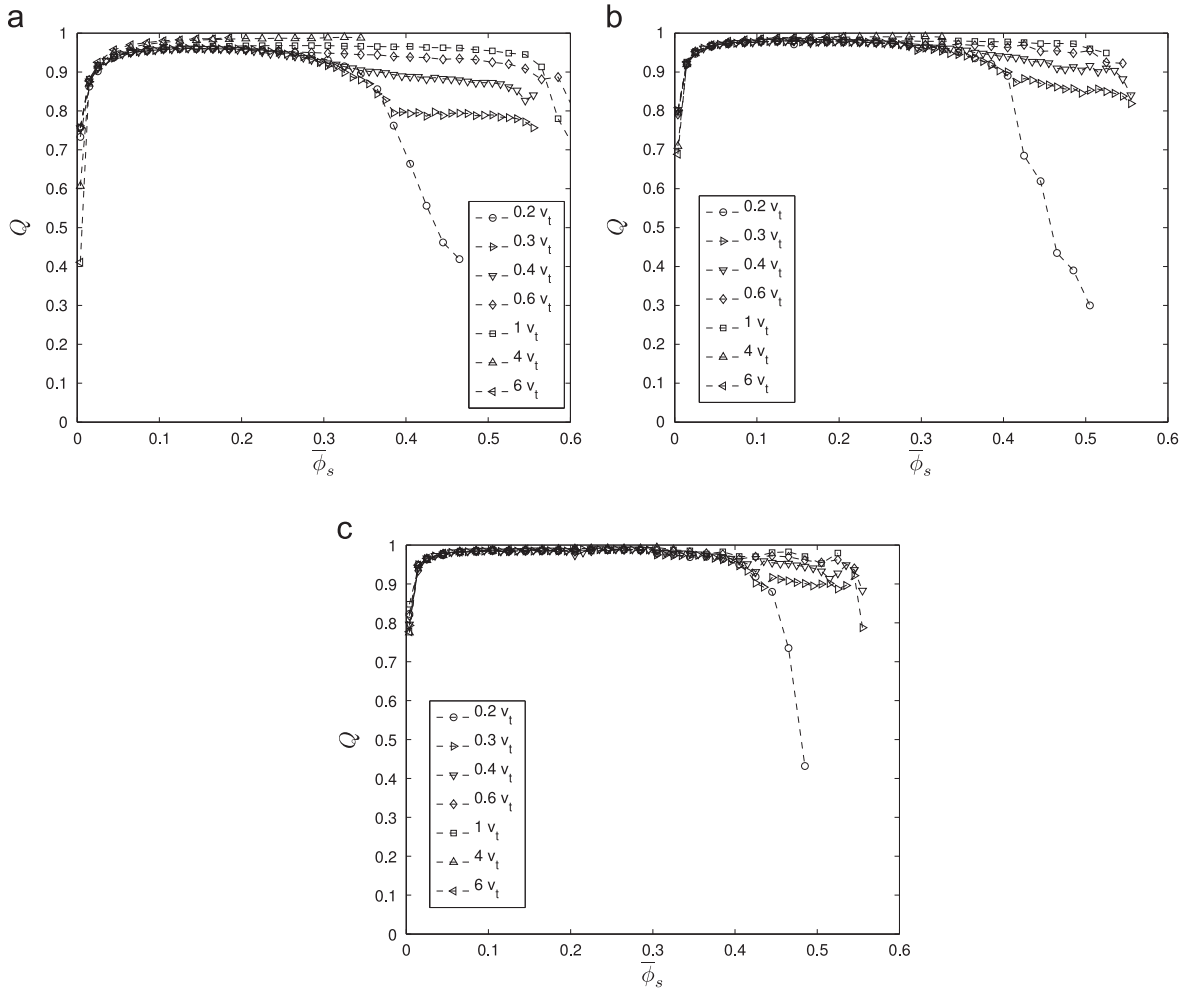

Fig. 6. Correction to the interphase heat transfer coefficient (Q) as a function of the filtered particle volume fraction ($\overline{\phi_s}$). Legend indicates filtered slip velocity in terms of the terminal velocity. Dimensionless filter size, $\hat{\Delta}$, is (a) 2.056 (1 cm), (b) 4.112 (2 cm), and (c) 8.224 (4 cm).

was varied between 2.056 and 32.896 (1–16 cm). Compared to the variation in the correction to the interphase drag, Q varies over a much narrower range, especially at lower $\overline{\phi_s}$. For $\overline{\phi_s} > 0.4$, while the range of Q is larger, it must be pointed out that most of the realizations are at the lower end of the range. Thus, even with a relatively small filter size, there is a substantial correction to the interphase heat transfer coefficient (except at the very dilute/dense regions). The range of variation implies a 1–2 orders of magnitude reduction in the interphase heat transfer coefficient, which is consistent with results reported by Kashyap and Gidaspow (2010, 2011) and Wang and Li (2005).

Fig. 6a shows the correction, Q, for $\hat{\Delta} = 2.056$ (1 cm) for different filtered slip velocity bins. The data are a subset of those in Fig. 5. While the microscopic interphase heat transfer coefficient is an increasing function of the slip velocity (Gunn, 1978), the filtered analog appears to have the opposite dependency with respect to the *filtered* slip velocity (similar behavior is seen for the filtered interphase drag coefficient in Milioli et al., to appear). This result is simply due to the effect of the sub filter-scale microstructure; the extent of heterogeneity increasing with increasing filtered slip velocity. These results suggest that, most of the variation in Q may be attributed to that in the filtered slip velocity. Furthermore, meaningful variation with respect to the filtered slip velocity is seen only for $\overline{\phi_s} > 0.3$. For very low filtered slip velocities ($< 0.4 v_t$), there is a pronounced drop in Q for $\overline{\phi_s} > 0.3$.

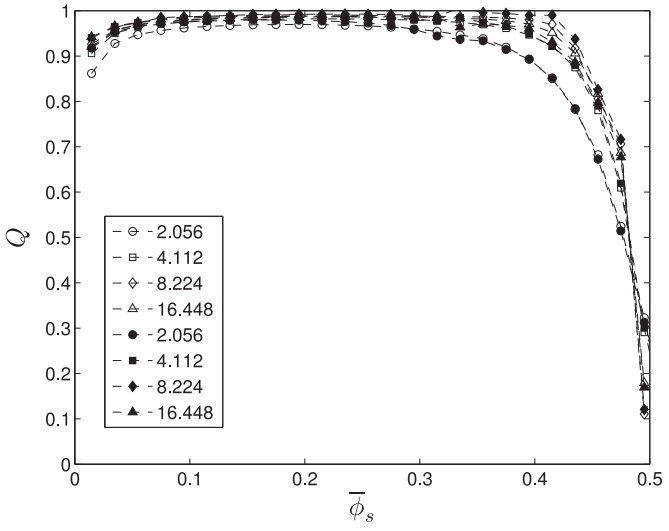

Fig. 7. Correction to the interphase heat transfer coefficient (Q) as a function of the filtered solids volume fraction ($\overline{\phi_s}$). Legend indicates dimensionless filter size. Open/Filled symbols correspond to a grid resolution of 1.25 mm/2.5 mm.

For larger filtered slip velocities, the correction does not drop meaningfully until $\overline{\phi_s} > 0.5$. Fig. 6b and c shows analogous results for $\hat{\Delta} = 4.112$ (2 cm) and $\hat{\Delta} = 8.224$ (4 cm), respectively. The

behavior seen in these figures is very similar to that seen in Fig. 6a. We notice that the sensitivity of Q with respect to the filtered slip velocity is negligible, except for $\overline{\phi_s} > 0.4$, and very low filtered slip velocities. With the further observation that most of the realizations for $\overline{\phi_s} > 0.4$ involve very low slip velocities, the results suggest that we may be able to formulate Q just in terms of $\overline{\phi_s}$ and $\hat{\Delta}$ by averaging over the filtered slip velocity dependence; these results are shown in Fig. 7. We see that the correction seems to approach an asymptotic envelope as $\hat{\Delta}$ exceeds 8.224 (4 cm). The correction is almost constant (~0.99) for over much of the range of $\overline{\phi_s}$, and rapidly approaches zero outside this interval. The variation of Q with respect to $\hat{\Delta}$ and $\overline{\phi_s}$ is captured quite well with the following fit:

$$Q = Q_1(\overline{\phi_s})Q_2(\hat{\Delta}) \tag{54}$$

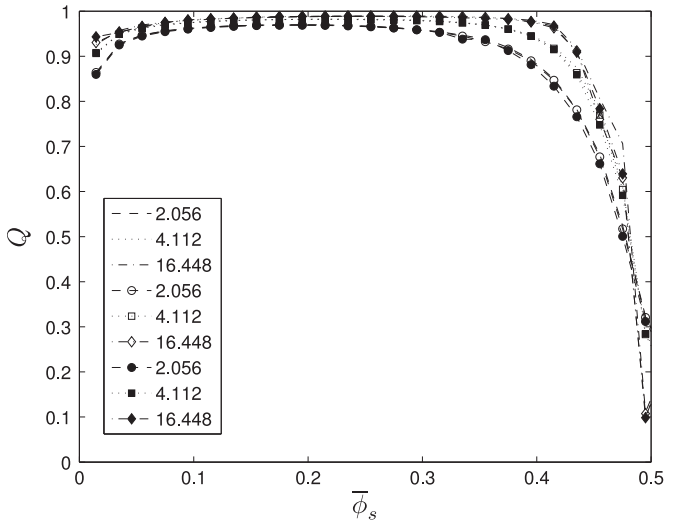

Fig. 8. Correction to the interphase heat transfer coefficient (Q) as a function of the filtered particle volume fraction ($\overline{\phi_s}$). Legend indicates dimensionless filter size. Dashed lines without symbols correspond to $e_p = 0.9$. Open/filled symbols correspond to $e_p = 0.85/0.95$.

$$Q_1(\overline{\phi_s}) = \begin{cases} \dfrac{0.9957\overline{\phi_s}}{\overline{\phi_s} + 0.0014} & \overline{\phi_s} \le 0.24 \\ \dfrac{0.9846\overline{\phi_s}^2 - 0.9739\overline{\phi_s} + 0.2408}{\overline{\phi_s}^2 - 0.9868\overline{\phi_s} + 0.2437} & 0.24 < \overline{\phi_s} \le 0.49 \\ 0 & \overline{\phi_s} > 0.49 \end{cases} \tag{55}$$

$$Q_2(\hat{\Delta}) = \begin{cases} \dfrac{\hat{\Delta}^3 - 2.0683\hat{\Delta}^2 + 0.4642\hat{\Delta}}{\hat{\Delta}^3 - 2.0436\hat{\Delta}^2 + 0.4518\hat{\Delta} - 0.039} & \hat{\Delta} > 0.257 \\ 0 & \hat{\Delta} \le 0.257 \end{cases} \tag{56}$$

Note that in our fine-grid simulations, the dimensionless grid size is 0.257 and as such $Q = 0$ by definition for $\hat{\Delta} = 0.257$. Therefore we have fit the function Q_2 to be zero for $\hat{\Delta} \le 0.257$. Q_2 rapidly approaches 1 as the filter size increases (Q_2~0.99 for $\hat{\Delta} = 3$). Thus, in all likelihood when simulating device scale flows, $Q \sim Q_1(\overline{\phi_s})$ will suffice as the choice for the correction to the interphase heat transfer coefficient; that is, the correction may be taken to be essentially independent of filter size.

Fig. 8 shows the effect of varying the coefficient of restitution on Q. It is quite clear that the results for the correction are insensitive in this respect, as was the case for the filtered thermal diffusivity. Finally, we wish to examine the sensitivity of the results with respect to a change in the correlation for the Nusselt number. Fig. 9 compares the results obtained for Q for the cases of Gunn's (1978) correlation and the case wherein the Nusselt number is set to a constant value ($Nu = 10$). While there is some variability in Q, the results for the correction are quite robust, and the fit for Q described earlier should suffice in practice.

7. Summary

We have extended filtered two-fluid models to accommodate *passive scalar transport* in gas–particle flows. Our calculations are based on fine-grid simulations of gas–particle flows (with the presence of a passive scalar) in a two-dimensional periodic domain and filtering the results. We have calculated the filtered intraphase transport coefficient (filtered diffusivity) and filtered interphase heat/mass transfer coefficient (or equivalently the filtered Nusselt/Sherwood number correlation). Eqs. (50)–(56) encapsulate the

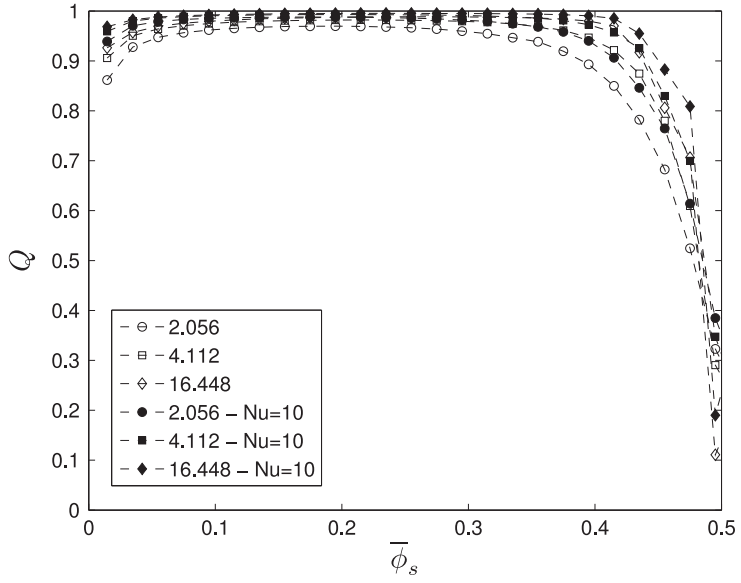

Fig. 9. Correction to the interphase heat transfer coefficient (Q) as a function of the filtered particle volume fraction ($\overline{\phi_s}$). Legend indicates dimensionless filter size. Filled symbols correspond to the case where Gunn's correlation for the Nusselt number is replaced with a constant Nusselt number value of 10.

specification of the filtered models for filtered diffusivity and the intraphase heat/mass transfer coefficient. We find that the filtered diffusivity may be cast into constitutive relations similar to Smagorinsky (1963) type models used in large-eddy simulation of scalar transport in single phase-turbulent flows. These results enable us to calculate the filtered Prandtl/Schmidt number.

The filtered interphase heat/mass transfer coefficient is cast in terms of a correction to the microscopic interphase heat/mass transfer coefficient. The correction is a function of the filter size, the filtered solids volume fraction, and the filtered slip velocity. However, the slip velocity dependence is such that the correction may be averaged with respect to this variable, leaving a function of filter size and filtered solids volume fraction. The correction is significant, even at filter sizes as small as 1 cm, and rapidly approaches an asymptotic envelope as the filter size is increased. We see a 1–2 orders of magnitude reduction in the interphase heat/mass transfer coefficient, which is consistent with that reported in the literature.

Future work of interest involves simulations in three-dimensional periodic domains (though the three-dimensional simulation results are found to be quite similar to those obtained from two-dimensional simulations for intraphase transport properties; see Igci and Sundaresan (2011b), and possibly improved prediction in the form of dynamic filtered models for intraphase and interphase transport. These type of models are used extensively in single phase turbulent flows (Germano et al., 1991) and have been recently adapted to gas–particle flows (Parmentier et al., 2011).

Notation

C_D	fluid–particle drag coefficient
C_{p_i}	specific heat capacity for phase i
d	particle diameter
e_p	coefficient of restitution of particle phase
$\boldsymbol{f_D}$	fluid–particle drag force
$\boldsymbol{g}$	gravitational acceleration vector
g_0	radial distribution function at contact
$G(\boldsymbol{x},\boldsymbol{y})$	weight function for filtering
$\boldsymbol{I}$	unit tensor
J_{coll}	collisional dissipation of granular energy
J_{vis}	viscous dissipation of granular energy
k_g	molecular conductivity of gas phase
k_s	effective conductivity of particle phase
Nu	Nusselt number
p_g	gas-phase pressure
Pr_g	Prandtl number for the gas phase
$Pr_{i_{filt}}$	Filtered Prandtl number for the phase i
$\boldsymbol{q}$	granular energy conduction vector
Q	correction to interphase heat transfer coefficient
Re_g	Reynolds number for the gas phase
$\boldsymbol{S}_i$	rate of deformation tensor for phase i
$\widetilde{\boldsymbol{S}}_i$	filtered rate of deformation tensor for phase i
$\hat{\widetilde{\boldsymbol{S}}}_i$	dimensionless rate of deformation tensor for phase i, $\hat{\widetilde{\boldsymbol{S}}}_i = \widetilde{\boldsymbol{S}}_i v_t/\lvert\boldsymbol{g}\rvert$
$\hat{s}_i$	dimensionless filtered scalar shear rate for phase i, $\hat{s}_i = \sqrt{2\hat{\widetilde{\boldsymbol{S}}}_i : \hat{\widetilde{\boldsymbol{S}}}_i}$
T_i	thermodynamic temperature of phase i
$\boldsymbol{v}_i$	velocity of phase i
v_t	terminal settling velocity of isolated particle
$\boldsymbol{x}$	generic spatial position vector
$\boldsymbol{y}$	generic spatial position vector

Greek letters

$\alpha_{i_{filt}}$	dimensional filtered thermal diffusivity for phase i
$\hat{\alpha}_{i_{filt}}$	dimensionless filtered thermal diffusivity for phase i $\hat{\alpha}_{i_{filt}} = \alpha_{i_{filt}}\lvert\boldsymbol{g}\rvert/v_t^3$
β	fluid–particle friction coefficient
γ	interphase heat transfer coefficient
γ_{filt}	filtered interphase heat transfer coefficient
Γ_{slip}	production of granular energy through interphase slip
δ	dimensional grid size
Δ	dimensional filter size
$\hat{\Delta}$	dimensionless filter size $\hat{\Delta} = \Delta\lvert\boldsymbol{g}\rvert/v_t^2$
λ	conductivity of granular energy
μ_b	bulk viscosity of particle phase
μ_g	molecular gas phase shear viscosity
μ_g^*	effective gas phase shear viscosity
μ_s	shear viscosity of particle phase
$\dot{\Pi}_s$	particle phase energy input rate
ρ_s	particle density
ρ_g	gas density
$\boldsymbol{\sigma}_i$	stress tensor for phase i
ϕ_i	volume fraction of phase i
$\langle\phi_s\rangle_d$	domain averaged particle phase volume fraction

Acknowledgements

SS acknowledges the financial support for this work from the Department of Energy Carbon Capture Simulation Initiative and ExxonMobil Research and Engineering Co. CCM and FEM are grateful for the financial support from the São Paulo Research Foundation – FAPESP (Brazil), which allowed them to pursue this research at Princeton University.

References

Agrawal, K., Loezos, P.N., Syamlal, M., Sundaresan, S., 2001. The role of meso-scale structures in rapid gas–solids flows. J. Fluid Mech. 445, 151.

Andrews IV, A.T., Loezos, P.N., Sundaresan, S., 2005. Coarse-grid simulation of gas–particle flows in vertical risers. Ind. Eng. Chem. Res. 44 (16), 6022.

Breault, R.W., 2006. A review of gas–solid dispersion and mass transfer coefficient correlations in circulating fluidized beds. Powder Technol. 163, 9.

Dong, W., Wang, W., Li, J., 2008a. A multiscale mass transfer model for gas–solid riser flows. Part I.: Sub-grid model and simple tests. Chem. Eng. Sci. 63, 2798.

Dong, W., Wang, W., Li, J., 2008b. A multiscale mass transfer model for gas–solid riser flows. Part II.: Sub-grid simulation of ozone decomposition. Chem. Eng. Sci. 63, 2811.

Fan, L.S., Zhu, C., 1998. Principles of Gas–Solid Flows. Cambridge University Press, Cambridge.

Gidaspow, D., 1994. Multiphase Flow and Fluidization: Continuum and Kinetic Theory Descriptions. Academic Press Inc., San Diego.

Germano, M., Piomelli, U., Moin, P., Cabot, W.H., 1991. A dynamic subgrid-scale eddy viscosity model. Phys. Fluids A 3, 1760.

Gunn, D.J., 1978. Transfer of heat or mass to particles in fixed and fluidised beds. Int. J. Heat Mass Transfer 21, 467.

Hansen, K.G., Solberg, T., Hjertager, B.H., 2004. A three-dimensional simulation of gas/particle flow and ozone decomposition is the riser of a circulating fluidized bed. Chem. Eng. Sci. 59, 5217.
Holloway, W., Sundaresan, S., 2012. Filtered models for reacting gas–particle flows. Chem. Eng. Sci. 82, 132.
Hsiau, S.S., Hunt, M.L., 1993. Shear-induced particle diffusion and longitudinal velocity fluctuations in a granular flow mixing layer. J. Fluid Mech. 151, 299.
Hunt, M.L., 1997. Discrete element simulations for granular material flows: effective thermal conductivity and self diffusivity. Int. J. Heat Mass Transfer 40, 3059.
Igci, Y., 2011. Closures for Coarse-grid Simulations of Fluidized Gas–Particle flows, Ph.D. Thesis, Princeton University, Princeton, NJ.
Igci, Y., Andrews IV, A.T., Sundaresan, S., O'Brien, T.J., 2008. Filtered two-fluid models for fluidized gas–particle suspensions. AIChE J. 54, 1431.
Igci, Y., Sundaresan, S., 2011a. Verification of filtered two-fluid models for gas–particle flow in risers. AIChE J. 57, 2691.
Igci, Y., Sundaresan, S., 2011b. Constitutive models for filtered two-fluid models of fluidized gas–particle flows. Ind. Eng. Chem. Res. 50, 13190.
Jackson, R., 2000. Dynamics of Fluidized Particles. Cambridge University Press, Cambridge, UK.
Kashyap, M., Gidaspow, D., 2010. Computation and measurements of mass transfer and dispersion coefficients in fluidized beds. Powder Technol. 203, 40.
Kashyap, M., Gidaspow, D., 2011. Measurement and computation of low mass transfer coefficients for FCC particles with ozone decomposition reaction. AIChE J. 58, 707.
Loezos, P.N., Sundaresan, S., 2002. The role of meso-scale structures on dispersion in gas–particle flows. In: Circulating Fluidized Beds VII, pp. 427–434.
Lun, C.K.K., Savage, S.B., Jeffrey, D.J., Chepurniy, N., 1984. Kinetic theories of granular flows: inelastic particles in Couette flow and slightly inelastic particles in a general flow field. J. Fluid Mech. 140, 223.
Milioli, C.C., Milioli, F.E., Holloway, W., Agrawal, K., Sundaresan, S. Filtered two-fluid models for fluidized gas–particle flows: new constitutive relations. AIChE J., to appear.
Moin, P., Squires, K., Cabot, W., Lee, S., 1991. A dynamic subgrid-scale model for compressible turbulence and scalar transport. Phys. Fluids A 3, 2746.
Parmentier, J.F., Simonin, O., Delsart, O., 2011. A functional subgrid drift velocity model for filtered drag prediction in dense fluidized bed. AIChE J. 58, 1084.
Pope, S.B., 2000. Turbulent Flows. Cambridge University Press, Cambridge, UK.
Rogers, M.M., Mansour, N.N., Reynolds, W.C., 1989. An algebraic model for the turbulent flux of a passive scalar. J. Fluid Mech. 203, 77.
Schmidt, A., Renz, U., 2000. Numerical prediction of heat transfer in fluidized beds by a kinetic theory of granular flows. Int. J. Therm. Sci. 39, 871.
Smagorinsky, J., 1963. General circulation experiments with the primitive equations. Mon. Weather Rev. 91, 99.
Syamlal, M., Rogers, W., O'Brien, T.J., 1993. MFIX Documentation Theory Guide.
Wang, L., Yang, N., Li, J., 2005. Multi-scale mass transfer model for gas–solid two-phase flow. Chem. Eng. Commun. 192, 1636.